The Journal of Chemical Physics

Point defects in crystals of charged colloids

Cite as: J. Chem. Phys. **154**, 164905 (2021); https://doi.org/10.1063/5.0047034
Submitted: 09 February 2021 . Accepted: 08 April 2021 . Published Online: 26 April 2021

Rinske M. Alkemade, Marjolein de Jager, Berend van der Meer, Frank Smallenburg, and Laura Filion

The Journal of Chemical Physics ARTICLE scitation.org/journal/jcp

Point defects in crystals of charged colloids

Cite as: J. Chem. Phys. 154, 164905 (2021); doi: 10.1063/5.0047034
Submitted: 9 February 2021 • Accepted: 8 April 2021 •
Published Online: 26 April 2021

Rinske M. Alkemade,[1] Marjolein de Jager,[1] Berend van der Meer,[2] Frank Smallenburg,[3] and Laura Filion[1,a)]

AFFILIATIONS

[1]Soft Condensed Matter, Debye Institute of Nanomaterials Science, Utrecht University, Utrecht, The Netherlands
[2]Department of Chemistry, Physical and Theoretical Chemistry Laboratory, University of Oxford, South Park Road, Oxford OX1 3QZ, United Kingdom
[3]Université Paris-Saclay, CNRS, Laboratoire de Physique des Solides, 91405 Orsay, France

[a)]**Author to whom correspondence should be addressed:** l.c.filion@uu.nl

ABSTRACT

Charged colloidal particles—on both the nano and micron scales—have been instrumental in enhancing our understanding of both atomic and colloidal crystals. These systems can be straightforwardly realized in the lab and tuned to self-assemble into body-centered-cubic (BCC) and face-centered-cubic (FCC) crystals. While these crystals will always exhibit a finite number of point defects, including vacancies and interstitials—which can dramatically impact their material properties—their existence is usually ignored in scientific studies. Here, we use computer simulations and free-energy calculations to characterize vacancies and interstitials in FCC and BCC crystals of point-Yukawa particles. We show that, in the BCC phase, defects are surprisingly more common than in the FCC phase, and the interstitials manifest as so-called crowdions: an exotic one-dimensional defect proposed to exist in atomic BCC crystals. Our results open the door to directly observe these elusive defects in the lab.

I. INTRODUCTION

Suspensions of charged colloids are among the most fundamental systems in colloidal science. These systems, consisting of charged colloidal spheres suspended in a solvent containing salt, which screens the Coulombic repulsions between the spheres, have been extensively studied using experiments, simulations, and theory.[1–15] In the case of single-component spherical colloids, the bulk phase behavior is extremely well understood, with impressive quantitative comparisons between theory and experiment.[4,5,13] These quantitative comparisons have been facilitated by the highly tunable nature of experimental systems of charged colloids.[8,16,17] From these studies we know that for sufficiently high densities or strongly charged particles, identically charged colloids self-assemble into one of two crystal structures, depending on the degree of screening. Broadly, for low salt concentrations, where the screening is weak, the system forms a body-centered-cubic (BCC) crystal, while high salt concentrations result in a face-centered-cubic (FCC) crystal.

In equilibrium, such crystalline phases always feature a finite concentration of defects. These defects, like vacancies and interstitials, can have a profound impact on the mechanical, optical, and electronic properties of crystalline materials. In the realm of colloid science, where the creation of new materials to manipulate light is one of the overarching goals, the presence of defects strongly affects optical properties.[18–20] It is, therefore, perhaps surprising that despite the massive body of literature on crystals formed by charged colloids, little is known about how defects manifest in their 3D crystalline phases.

In three dimensions, some of the earliest work on defects in colloidal crystals focused on point defects (vacancies and interstitials) in single-component hard-sphere crystals.[21–23] This colloidal model system forms an FCC crystal, with relatively few point defects in equilibrium: at melting, the crystal is predicted to have approximately 10^{-4} vacancies and 10^{-8} interstitials per lattice site. Subsequent studies have explored, e.g., the local structural impact of defects,[24–26] the diffusion of vacancies and interstitials,[25,27] and the emergence of stacking faults[28–31] in hard-sphere systems. However, in general, defects in 3D colloidal crystals have received relatively little attention due to, at least in part, the expectation that they do not occur in large quantities in equilibrium.

A notable exception is the relatively recent prediction that simple cubic crystals of repulsive particles frequently exhibit large

numbers (≈0.06 per lattice site) of vacancies that are spread over a row of lattice sites in one dimension.[32–34] These 1D vacancies, predicted for simple cubic crystals, are reminiscent of so-called interstitial crowdions. This intriguing type of interstitial defect was proposed by Paneth in 1950[35] to explain anomalous self-diffusion in BCC crystals of alkali metals. In this picture, the defect is expected to spread out over multiple lattice sites arranged along a one-dimensional line, resulting in preferential diffusion along that direction. In the atomic realm, explorations of these defects have been largely focused on simulations,[36–40] and simple theoretical models have been used to capture their behavior.[41–46]

To date, an analog to these defects in a colloidal realization of a BCC crystal—which would allow for direct observation in real time using, e.g., confocal microscopy—is lacking. It is therefore intriguing to explore how interstitials manifest in colloidal BCC crystals and, in particular, in systems that can be directly, and even quantitatively, reproduced in an experimental setting.

Here, we use computer simulations to explore both the concentration and structure of point defects in BCC and FCC crystals of one of the most fundamental models for screened charged particles—the point Yukawa model. Our results predict that this fundamental system forms a direct colloidal realization of crowdion interstitials in BCC crystals. Moreover, we find that BCC exhibits significantly higher concentrations of point defects and, hence, expect that these crowdions play an important role in controlling the material properties of the crystal. Importantly, given the substantial concentration of crowdions predicted to occur in equilibrium, our results pave the way for directly observing these rare and elusive defects in colloidal experiments.

II. MODEL

We consider a system of N charged colloids of diameter σ suspended in a solvent containing ions characterized by an inverse Debye screening length κ_D and Bjerrum length λ_B. Within Derjaguin–Landau–Verwey–Overbeek (DLVO) theory, the effective potential between the colloids is given by

$$\beta\phi(r) = \frac{\varepsilon}{r} e^{-\kappa_D r}, \tag{1}$$

where

$$\varepsilon = \frac{Z^2 \lambda_B e^{\kappa_D \sigma}}{(1+\kappa\sigma/2)^2}, \tag{2}$$

with Z being the charge of the colloids in electron charges, and $\beta = 1/k_B T$, with k_B being the Boltzmann constant and T being the temperature. Note that the so-called Yukawa potential not only describes charged colloids but also has been widely applied in the study of dusty plasmas.[47]

Conveniently, the phase behavior of this system can be fully characterized by two dimensionless parameters, namely,

$$\Gamma = \frac{\varepsilon}{a k_B T},$$
$$\kappa = a\kappa_D,$$

with $a = \left(\frac{4\pi N}{3V}\right)^{-\frac{1}{3}}$ being the Wigner–Seitz radius.

The phase diagram for this system has been explored extensively using theory, simulations, and experiments. In Fig. 1, we show the phase behavior using the phase boundaries approximated in Refs. 6 and 7. It consists of a fluid phase and two crystal phases: face-centered-cubic (FCC) and body-centered-cubic (BCC), with all phase boundaries corresponding to first-order phase transitions. Note that the coexistence regions here are all small and have been simply presented as lines, similar to Refs. 6 and 7. In this paper, we will explore the behavior of point defects associated with the crystals that appear in this 2D phase diagram.

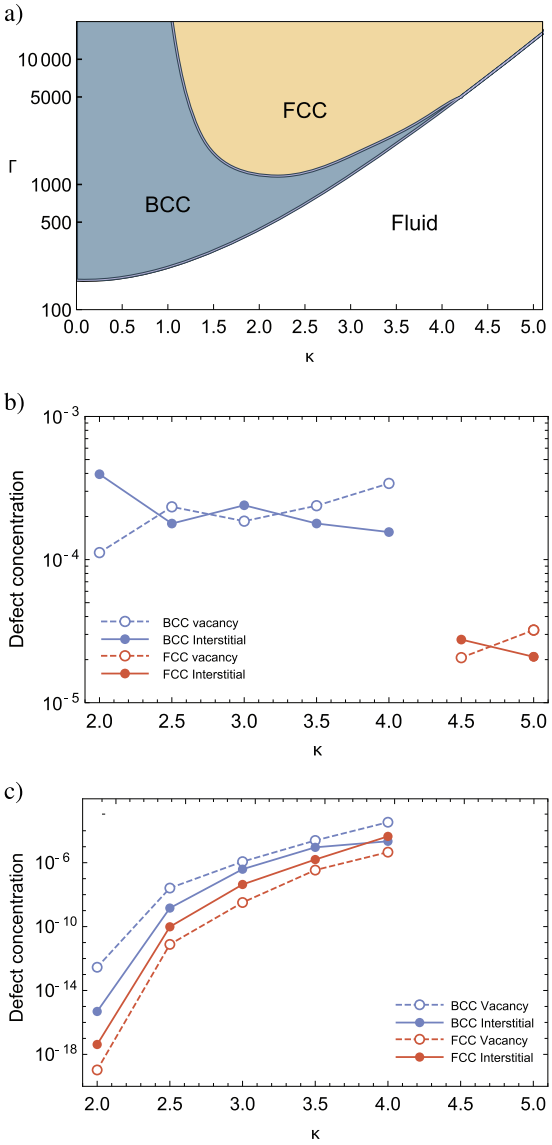

FIG. 1. (a) Phase diagram of Yukawa systems in the (κ, Γ) plane, with the phase boundaries from Refs. 6 and 7. Vacancy and interstitial concentrations plotted along (b) the fluid–crystal phase boundary and (c) the BCC–FCC phase boundary. We estimate an error of up to $0.2k_BT$ in our calculation of the $\mu^{\text{vac(int)}}$, leading to an approximate error of a factor of 1.2 in the concentrations.

III. METHODS

A. General simulation details

We used Monte Carlo simulations in the NVT-ensemble with periodic boundary conditions,[48] where the particles interact via the point Yukawa potential [Eq. (1)]. The potential was truncated and shifted such that the shift was never more than $10^{-5}k_BT$. The system size was always chosen to be large enough to accommodate this choice such that the cutoff range is less than half the box length.

The system sizes were chosen depending on the phase in question. For studying defect concentrations, we used systems containing between 250 and 1500 particles. For select points of the smallest systems, we examined whether doubling the system size mattered, and in all cases, it had no discernible effect on the defect concentrations. For studying the shape of the defects, we used a system ranging from 1000 to 3500 particles and again ensured that the system size was not affecting the results.

B. Concentration of defects

To determine the vacancy concentration, we make the assumption that the defect concentration is sufficiently low that (i) the defects do not interact and (ii) the equation of state of the crystal is unaffected by the presence of defects. In this case, the free energy of a system of N particles in a volume V at temperature T can be written as

$$\beta F^{\text{vac}}(N,V,T) = \beta M f^{\text{df}}(N,V,T) + \beta(M-N)f^{\text{vac}} + N\log\frac{N}{M} + (M-N)\log\frac{M-N}{M}, \tag{3}$$

where $M > N$ is the number of lattice sites, f^{df} is the free energy per particle of the defect-free crystal, and f^{vac} is the free energy associated with creating a single vacancy at a specific lattice site.

Taking the Legendre transform to turn this Helmholtz free energy into a Gibbs free energy and minimizing with respect to the number of lattice sites M, we find that the equilibrium concentration of vacancies is given by

$$\langle n_{\text{vac}}\rangle \equiv \left\langle \frac{M-N}{N} \right\rangle = \exp[-\beta\mu^{\text{vac}}], \tag{4}$$

where μ^{vac} is defined as $f^{\text{vac}}(\rho_M, T) + \mu^{\text{df}}(P, T)$, with $\mu^{\text{df}}(P, T)$ being the chemical potential of a defect-free crystal and $\rho_M = M/V$ being the density of lattice sites. Note that P is the pressure.

For a crystal containing interstitials, where $M < N$, we use a similar approach yielding an equilibrium concentration of interstitials,

$$\langle n_{\text{int}}\rangle \equiv \left\langle \frac{N-M}{N} \right\rangle = \exp[-\beta\mu^{\text{int}}], \tag{5}$$

with $\mu^{\text{int}} = f^{\text{int}}(\rho_M, T) - \mu^{\text{df}}(P, T)$. Here, $f^{\text{int}}(\rho_M, T)$ is the free energy associated with creating an interstitial at a specific lattice site. In order to obtain the concentration of point defects for various points along the phase boundary of the Yukawa crystal, we thus need to measure $f^{\text{vac}}(\rho_M, T)$, $f^{\text{int}}(\rho_M, T)$, and $\mu^{\text{df}}(P, T)$ in a Yukawa crystal. Because it is not possible to measure these free energies directly in a Monte Carlo simulation, we use thermodynamic integration as described below.

To obtain the chemical potential μ^{df} of the defect-free crystals, we first use the Frenkel–Ladd method[49] to obtain the Helmholtz free energy. We then combine this with the pressure, measured via the virial expression,[48] to determine the chemical potential.

We now turn our attention to the method for finding the free energies $f^{\text{int}}(\rho_M, T)$ and $f^{\text{vac}}(\rho_M, T)$ associated with creating point defects. In the case of a vacancy, we break f^{vac} up into two contributions: $f^{\text{vac}} = f^{\text{shrink}} + f^{\text{remove}}$, where f^{shrink} is associated with turning one of the particles of a defect-free crystal into a non-interacting particle and f^{remove} is associated with removing this non-interacting particle. Similarly, in the case of an interstitial, we first compute the free energy, f^{add}, associated with inserting a non-interacting particle and then calculate the free energy, f^{grow}, associated with turning this non-interacting particle into a normal-interacting particle. Note that in all cases, the particle associated with a defect is confined to a single Wigner–Seitz cell.

We then calculate the total free energy for the interstitial using $f^{\text{int}} = f^{\text{grow}} + f^{\text{add}}$. The free energies associated with f^{add} and f^{remove} are given by

$$f^{\text{add}} = -k_BT\ln\left(\frac{V^{WS}}{\Lambda^3}\right) \tag{6}$$

and

$$f^{\text{remove}} = k_BT\ln\left(\frac{V^{WS}}{\Lambda^3}\right), \tag{7}$$

where V^{WS} is the volume of the Wigner–Seitz cell and Λ is the thermal de Broglie wavelength.

To calculate f^{shrink}, we use thermodynamic integration with an auxiliary Hamiltonian,

$$U_\lambda = \lambda U_0 + (1-\lambda)U_{\text{non-int}}, \tag{8}$$

with U_0 being the normal interaction potential of our system and $U_{\text{non-int}}$ the potential energy of a system where one particle is non-interacting. Following standard thermodynamic integration, the free-energy difference between a crystal with one non-interacting particle and a defect-free crystal is then given by

$$f^{\text{shrink}} = F^{\text{non-int}} - F^{\text{df}} = -\int_0^1 d\lambda\langle U_{\text{non-int}} - U_0\rangle_\lambda, \tag{9}$$

with $F^{\text{non-int}}$ being the Helmholtz free energy of a crystal containing one non-interacting particle. The ensemble average, $\langle\cdots\rangle_\lambda$, is evaluated using the auxiliary potential given in Eq. (8). The free energy f^{grow} is determined following the same method. Note that in both cases, we evaluate the integral numerically using 34 different values of λ.

However, while in theory this method works fine, in practice, the sampling can become very slow. When the system is at $\lambda = 0$, we evaluate the energy difference in Eq. (9) using the potential $U_{\lambda=0} = U_{\text{non-int}}$. This means that without any energy penalty, the non-interacting particle can come very close to other particles if those particles are near their Wigner–Seitz cell boundary. Because we compute the potential energy difference with the system where

our particle does have interactions, the term $\langle U_{\text{non-int}} - U_0 \rangle_{\lambda=0}$ can become very large—in the interstitial case, even infinitely large. Due to these large energy differences, the simulation needs a long time to get a reliable answer for the value $\langle U_{\text{non-int}} - U_0 \rangle_{\lambda=0}$.

To circumvent this problem, we alter the potential. Instead of letting it diverge at $r = 0$ as it normally would do, we assume that the potential increases linearly below a certain defined value r_{alter}. By doing so, the potential has a finite value, U_{max}, at $r = 0$. If we evaluate $\langle U_{\text{non-int}} - U_0 \rangle_{\lambda=0}$ for higher λ values, this altered potential will not have any influence as the particles will never have a distance r with $r < r_{\text{alter}}$ due to the energy penalty. However, for small λ, we avoid the large energies. Because in the end, we integrate over the energy difference [see Eq. (9)], this alteration to the potential has no influence on the final free energy. We find that the precise values for U_{max} and r_{alter} do not matter as long as we make sure r_{alter} is sufficiently small that for higher values of λ, r will almost never be smaller than r_{alter}. We checked this by running the same simulation twice for different values of U_{max} and r_{alter}.

IV. RESULTS

We start our investigation by exploring the equilibrium concentration of vacancies and interstitials in both crystals. As a starting point, we focus on state points in the vicinity of the fluid–crystal phase boundary—the region on the phase diagram that is expected to have the highest concentration of defects. To predict these concentrations, we make the assumption that the defects do not interact and that their effect on the pressure of the system is negligible. We can then use a combination of Monte Carlo simulations and thermodynamic integration to extract the defect concentrations. The result is shown in Fig. 1(b).[50]

Clearly, along the fluid–crystal line, BCC appears to have more defects of both types than FCC. More specifically, for BCC, both the vacancy and interstitial concentrations are on the order of 10^{-4}, while for FCC, the concentrations are closer to 10^{-5}. For vacancies, these concentrations are similar to those found for hard spheres at coexistence (10^{-4}).[22] However, the interstitial concentration in both cases is orders of magnitude higher than the 10^{-8} predicted for interstitials in hard-sphere crystals at the fluid–crystal phase boundary.[22]

To make a more direct comparison of the behavior of the two crystals, we then calculated the defect concentrations along the FCC–BCC phase line. From Fig. 1(c), we observe again that BCC generally has more defects than FCC; while the difference in the interstitial concentration is small, the difference in the vacancy concentration varies from two to eight orders of magnitude. Clearly, BCC generally exhibits more equilibrium point defects than FCC.

To explore the large differences we observe between FCC and BCC, we now turn our attention to the structure of the point defects in these two crystals. To determine the structure, we performed *NVT* MC simulations with a single vacancy or interstitial present. To prevent the defect from hopping during our analysis, we confined all particles to their Wigner–Seitz cells[32,51] and then measured the average location of each particle during the simulation.

The results for a vacancy in FCC are shown in Figs. 2(a) and 2(b), while Figs. 2(e) and 2(f) depict the average deformation associated with a vacancy in a BCC crystal. In both crystals, as

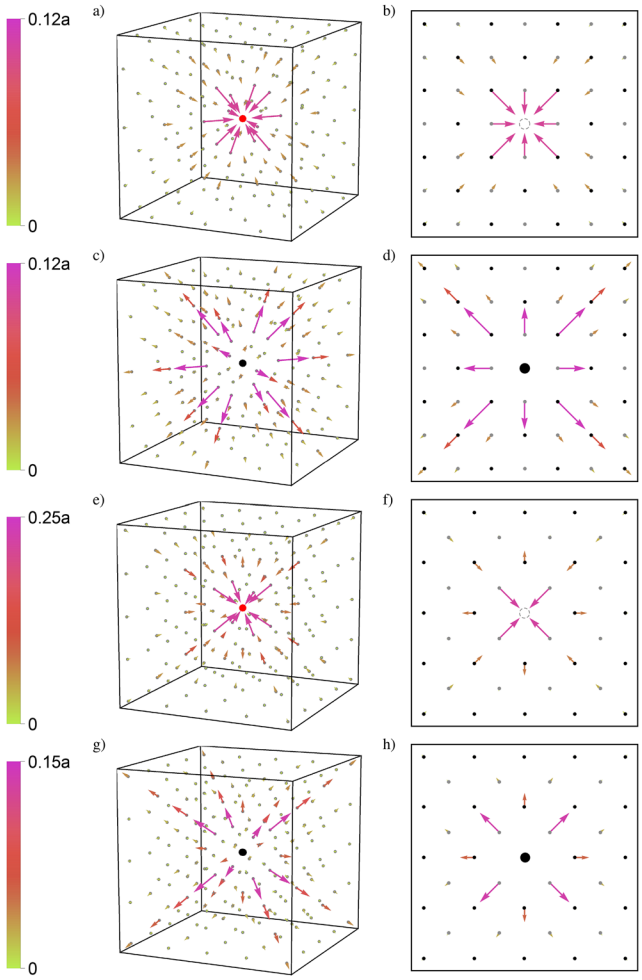

FIG. 2. Average lattice deformation due to a point defect in (a)–(d) the FCC crystal at $\kappa = 3.5$ and $\Gamma = 2565$ and (e)–(h) the BCC crystal at $\kappa = 3.5$ and $\Gamma = 2400$. (a), (b) and (e), (f) Deformation due to a vacancy (indicated by red or a dotted sphere) and (c) and (d) and (g) and (h) deformation due to an interstitial (indicated by a black sphere). Left: 3D representation of part of the simulation box. The gray points represent the lattice sites. Right: projection of the displacement vectors on two (100) planes on top of each other. The black points represent the lattice sites that lie in the plane of the defect and the gray points denote the lattice sites in the neighboring plane. In all panels, the size of the arrows is exaggerated, but the color of the arrows indicates the deformation in terms of the Wigner–Seitz radius a.

expected, the largest deformation is associated with the first shell of neighbors—however, it is approximately twice as large in the case of the BCC crystal (note the different scaling on the color bars). This likely arises due to the lower number of particles in the first shell of BCC, 8 in comparison to the 12 in FCC. In the BCC crystal, the particles are less strongly caged by their neighbors and are, hence, more free to move into the space opened up by the vacancy. More interesting is the behavior of the second shell of neighbors. While in FCC all particles again deviate in the direction of the vacancy, in BCC half the particles move toward the vacancy while the other

half move away from the defect. The end result is a much larger change in energy of the crystal upon removing the particle: in the system shown in Fig. 2, the average difference is $\beta\Delta U_{\mathrm{FCC}} = -35.6$ and $\beta\Delta U_{\mathrm{BCC}} = -42.9$ in the FCC and BCC crystals, respectively. This difference contributes directly to the difference in free-energy cost for creating a vacancy in the two crystals. In short, the BCC structure is better able to take advantage of the vacancy to reduce its local potential energy, which helps to alleviate the cost of creating a vacancy and, hence, makes them more prevalent.

The interstitials turn out to be an even more interesting case. In Figs. 2(c), 2(d), 2(g), and 2(h), we plot the average displacement of particles from their lattice sites in FCC and BCC crystals, respectively. In comparison to the vacancy case, these defects appear at first rather similar: in both crystals, the average deviations due to the interstitial are mainly along the lines pointing along the nearest-neighboring directions and decay slowly through a number of neighboring shells. In the FCC crystal, this means that particles lying along the six ⟨110⟩ lines are displaced the most, similar to what was found in hard-sphere crystals.[25] In the BCC crystals, it is the particles lying along the four ⟨111⟩ lines.

Interestingly, however, the averaged displacements do not tell the full story. If we examine the instantaneous realization of an interstitial, there is a spontaneous symmetry breaking in the displacement of neighboring particles along different directions, especially in the case of BCC. One clear way of demonstrating this is to quench a system containing an interstitial to high values of Γ such that the system minimizes its potential energy. As shown in Fig. 3, this quench has a particularly remarkable effect on the BCC crystal. While in the case of FCC [Fig. 3(a)], the defect takes on a normal dumbbell structure with a 3D displacement field around it, in BCC, the defect becomes one-dimensional [Fig. 3(b)]: only particles along one of the four ⟨111⟩ lines are displaced significantly. With this knowledge in mind, we can recalculate the average displacement field for an interstitial by first rotating each configuration so that the defect is always oriented along the same axis. The result is shown in Fig. 3 for the quenched system and in Fig. 4 for the system at finite Γ.

This one-dimensional configuration strongly resembles a so-called crowdion: an exotic 1D defect proposed to exist in some metallic BCC crystals.[35] In order to characterize the structure of the defects, we measure the average particle displacements $u_n = x_n - a_{111}n$ near the interstitials along the defect direction, where x_n is the position of particle n along the defect and a_{111} is the crystal lattice spacing along the ⟨111⟩ direction. We choose $n = 0$ to correspond to the particle just before the defect center and use "standard" boundary conditions: $u_{n=-\infty} = a_{111}$ and $u_{n=\infty} = 0$. We plot this displacement field for a BCC crystal with $\kappa = 3.5$ and $\Gamma = 2400$ in Fig. 4, along with the displacement field along the three other ⟨111⟩ lines. Clearly, particle positions along the defect direction are strongly affected by the presence of the interstitial, while along the other ⟨111⟩ directions, they remain essentially unperturbed—indicating that the defect is one-dimensional.

A classic characteristic of a crowdion is that the defect shape can be well captured by the Frenkel–Kontorova model.[41,45] This model describes a one-dimensional chain of particles that are connected to their neighbors via springs and embedded in a periodic external potential. Defects are included as missing or extra particles with respect to the number of external periodic wells. In the continuum limit, the average particle positions near a defect follow the soliton solution to the sine-Gordon equation, which has a single free parameter that captures the extent of the defect. Hence, to further confirm that the interstitials are realizations of crowdions, we compare our results to the soliton solution of the sine-Gordon equation [black dashed line in Fig. 4(b)] using the extension of the defect as a fit parameter. We observe excellent agreement. Curious as to how the shape of the defect is dependent on where we are on the phase diagram, we performed the same analysis for a range of different state points with different values of κ and Γ. Remarkably, in the area of the phase diagram close to the melting line, we see very little effect of either parameter on the structure of the

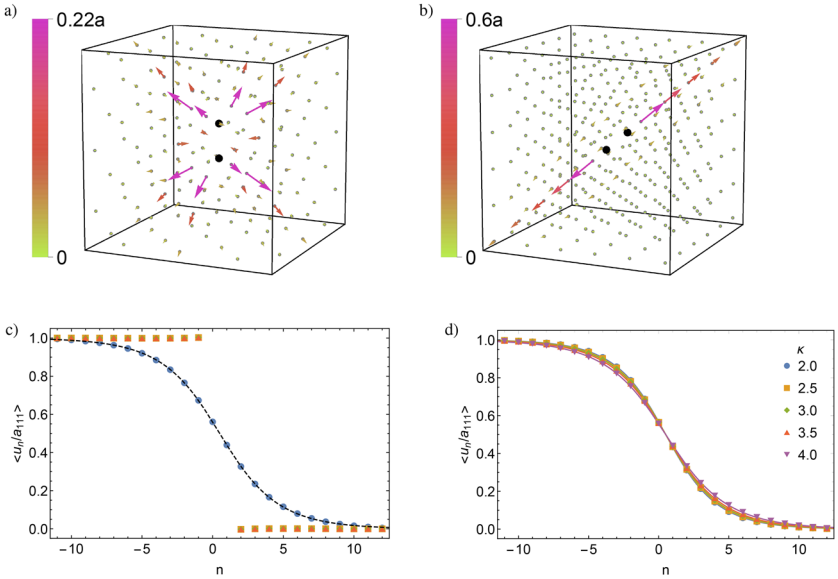

FIG. 3. Quenched lattice deformation due to an interstitial in (a) the FCC crystal and (b) the BCC crystal, both at $\kappa = 3.5$. The gray points represent the lattice sites of part of the simulation box, and the black spheres represent the actual positions of the interstitial and its companion. The size of the arrows is exaggerated, but the color of the arrows indicates the deformation in terms of the Wigner–Seitz radius a. (c) Displacement u_n along the four ⟨111⟩ directions for the same system as (b). The blue dots indicate u_n along the direction of the crowdion, and the dashed line represents the corresponding fitted soliton solution. (d) u_n along the direction of the crowdion for five different κ. The lines represent the corresponding fitted soliton solutions.

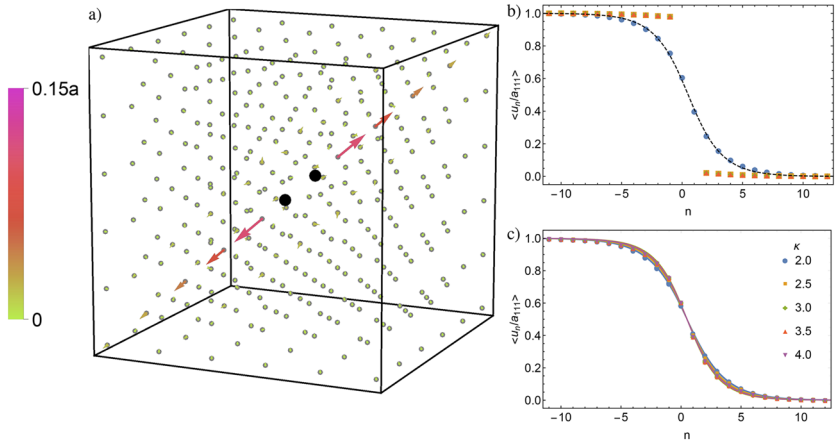

FIG. 4. (a) Lattice deformation due to an interstitial in the BCC crystal at $\kappa = 3.5$ and $\Gamma = 2400$. The gray points represent the lattice sites of part of the simulation box, and the black spheres represent the positions of the interstitial and its companion. The size of the arrows is exaggerated, but the color of the arrows indicates the deformation in terms of the Wigner–Seitz radius a. Note that these deformations are averaged over multiple configurations, which have been rotated so that the defect always points along the same direction. (b) Displacement u_n along the four ⟨111⟩ directions for the same system as (a). The blue dots indicate u_n along the direction of the crowdion, and the dashed line represents the corresponding fitted soliton solution. (c) u_n along the direction of the crowdion for $\kappa = 2.0$ and $\Gamma = 1000$, 1100, and 1205 (blue dots); $\kappa = 2.5$ and $\Gamma = 1000$, 1100, and 1205 (yellow squares); $\kappa = 3.0$ and $\Gamma = 1205$, 1400, and 1600 (green diamonds); $\kappa = 3.5$ and $\Gamma = 2200$, 2300, and 2400 (orange triangles); and $\kappa = 4.0$ and $\Gamma = 4000$, 4100, and 4200 (purple triangles). The lines represent the corresponding fitted soliton solutions.

crowdion. In Fig. 4(c), we show the displacement fields along the defect axis for 15 different state points and obtain essentially the same curve every time. This indicates that in this regime, the extension of the defect is largely independent of both the interaction strength and screening parameter. We note, however, that the crowdions do slowly get longer as Γ is increased far beyond the melting point. This can be observed from the shape of the quenched defects, as shown in Fig. 3(d).

V. CONCLUSIONS

In summary, we have characterized the point defects that appear in crystals of charged colloids, an archetypical colloidal model system. Surprisingly, we found dramatic differences between the two—fairly similar—crystal phases FCC and BCC. As a first observation, the BCC crystals contain dramatically more vacancies, as well as more interstitials, than their FCC counterparts. One logical explanation for this is the relatively small number of nearest-neighbors in the BCC crystals, which makes it easier for particles to partially emerge from their cages and make use of the extra room opened up by a vacancy—or adapt to the encroachment of a nearby interstitial.

Not only BCC exhibits significantly more defects but its interstitials manifest as exotic one-dimensional defects called crowdions.[35] The delocalized nature of such defects would be expected to promote fast and strongly anisotropic diffusion of the defects through the crystal.[36,39,40,45] In combination with the relatively large concentration of interstitials in BCC near melting, these defects are expected to strongly impact the transport properties of the crystal, including self-diffusion and the diffusion of dopants.[52]

The observation of a crowdion defect in an easy-to-realize and highly tunable colloidal system is important not only for our understanding of this system itself but also for understanding the nature of crowdions. In atomic systems, crowdions are both rare and hard to observe directly (almost all studies are based on simulations and theory[36–40,45]). In contrast, charged colloids can be studied in real space and real time using, e.g., confocal microscopy and, hence, are an ideal experimental playground for studying these defects.

Surprisingly, despite decades of intense studies, it appears that this fundamental colloidal model system has not yet given up all of its secrets.

ACKNOWLEDGMENTS

The authors thank Alfons van Blaaderen, Anna Nikolaenkova, and Emanuele Boattini for many useful discussions. L.F. acknowledges funding from the Dutch Research Council (NWO) for a Vidi grant (Grant No. VI.VIDI.192.102). B.v.d.M. acknowledges funding from the Rubicon research program with Project No. 019.191EN.011, which is financed by NWO.

DATA AVAILABILITY

The data that support the findings of this study are available from the corresponding author upon reasonable request.

REFERENCES

[1] S. Alexander, P. M. Chaikin, P. Grant, G. J. Morales, P. Pincus, and D. Hone, "Charge renormalization, osmotic pressure, and bulk modulus of colloidal crystals: Theory," J. Chem. Phys. **80**, 5776–5781 (1984).
[2] K. Kremer, M. O. Robbins, and G. S. Grest, "Phase diagram of Yukawa systems: Model for charge-stabilized colloids," Phys. Rev. Lett. **57**, 2694 (1986).
[3] M. O. Robbins, K. Kremer, and G. S. Grest, "Phase diagram and dynamics of Yukawa systems," J. Chem. Phys. **88**, 3286–3312 (1988).

[4]Y. Monovoukas and A. P. Gast, "The experimental phase diagram of charged colloidal suspensions," J. Colloid Interface Sci. **128**, 533–548 (1989).
[5]E. B. Sirota, H. D. Ou-Yang, S. K. Sinha, P. M. Chaikin, J. D. Axe, and Y. Fujii, "Complete phase diagram of a charged colloidal system: A synchrotron x-ray scattering study," Phys. Rev. Lett. **62**, 1524 (1989).
[6]S. Hamaguchi, R. T. Farouki, and D. H. E. Dubin, "Triple point of Yukawa systems," Phys. Rev. E **56**, 4671 (1997).
[7]A.-P. Hynninen and M. Dijkstra, "Phase diagram of hard-core repulsive Yukawa particles with a density-dependent truncation: A simple model for charged colloids," J. Phys.: Condens. Matter **15**, S3557 (2003).
[8]A. Yethiraj and A. van Blaaderen, "A colloidal model system with an interaction tunable from hard sphere to soft and dipolar," Nature **421**, 513–517 (2003).
[9]M. F. Hsu, E. R. Dufresne, and D. A. Weitz, "Charge stabilization in nonpolar solvents," Langmuir **21**, 4881–4887 (2005).
[10]C. P. Royall, M. E. Leunissen, A.-P. Hynninen, M. Dijkstra, and A. van Blaaderen, "Re-entrant melting and freezing in a model system of charged colloids," J. Chem. Phys. **124**, 244706 (2006).
[11]D. El Masri, P. van Oostrum, F. Smallenburg, T. Vissers, A. Imhof, M. Dijkstra, and A. van Blaaderen, "Measuring colloidal forces from particle position deviations inside an optical trap," Soft Matter **7**, 3462–3466 (2011).
[12]F. Smallenburg, N. Boon, M. Kater, M. Dijkstra, and R. van Roij, "Phase diagrams of colloidal spheres with a constant zeta-potential," J. Chem. Phys. **134**, 074505 (2011).
[13]T. Kanai, N. Boon, P. J. Lu, E. Sloutskin, A. B. Schofield, F. Smallenburg, R. van Roij, M. Dijkstra, and D. A. Weitz, "Crystallization and reentrant melting of charged colloids in nonpolar solvents," Phys. Rev. E **91**, 030301 (2015).
[14]S. Arai and H. Tanaka, "Surface-assisted single-crystal formation of charged colloids," Nat. Phys. **13**, 503–509 (2017).
[15]M. Chaudhuri, E. Allahyarov, H. Löwen, S. U. Egelhaaf, and D. A. Weitz, "Triple junction at the triple point resolved on the individual particle level," Phys. Rev. Lett. **119**, 128001 (2017).
[16]K. van Gruijthuijsen, M. Obiols-Rabasa, M. Heinen, G. Nägele, and A. Stradner, "Sterically stabilized colloids with tunable repulsions," Langmuir **29**, 11199–11207 (2013).
[17]T. E. Kodger, R. E. Guerra, and J. Sprakel, "Precise colloids with tunable interactions for confocal microscopy," Sci. Rep. **5**, 14635 (2015).
[18]Q. Yan, A. Chen, S. J. Chua, and X. S. Zhao, "Incorporation of point defects into self-assembled three-dimensional colloidal crystals," Adv. Mater. **17**, 2849–2853 (2005).
[19]R. Rengarajan, D. Mittleman, C. Rich, and V. Colvin, "Effect of disorder on the optical properties of colloidal crystals," Phys. Rev. E **71**, 016615 (2005).
[20]E. C. Nelson, N. L. Dias, K. P. Bassett, S. N. Dunham, V. Verma, M. Miyake, P. Wiltzius, J. A. Rogers, J. J. Coleman, X. Li *et al.*, "Epitaxial growth of three-dimensionally architectured optoelectronic devices," Nat. Mater. **10**, 676–681 (2011).
[21]C. H. Bennett and B. J. Alder, "Studies in molecular dynamics. IX. Vacancies in hard sphere crystals," J. Chem. Phys. **54**, 4796–4808 (1971).
[22]S. Pronk and D. Frenkel, "Point defects in hard-sphere crystals," J. Phys. Chem. B **105**, 6722–6727 (2001).
[23]S. Pronk and D. Frenkel, "Large effect of polydispersity on defect concentrations in colloidal crystals," J. Chem. Phys. **120**, 6764–6768 (2004).
[24]N. Y. C. Lin, M. Bierbaum, P. Schall, J. P. Sethna, and I. Cohen, "Measuring nonlinear stresses generated by defects in 3D colloidal crystals," Nat. Mater. **15**, 1172–1176 (2016).
[25]B. van der Meer, M. Dijkstra, and L. Filion, "Diffusion and interactions of point defects in hard-sphere crystals," J. Chem. Phys. **146**, 244905 (2017).
[26]B. VanSaders, J. Dshemuchadse, and S. C. Glotzer, "Strain fields in repulsive colloidal crystals," Phys. Rev. Mater. **2**, 063604 (2018).
[27]C. H. Bennett and B. J. Alder, "Persistence of vacancy motion in hard sphere crystals," J. Phys. Chem. Solids **32**, 2111–2122 (1971).
[28]J. P. Hoogenboom, D. Derks, P. Vergeer, and A. van Blaaderen, "Stacking faults in colloidal crystals grown by sedimentation," J. Chem. Phys. **117**, 11320–11328 (2002).
[29]S. Pronk and D. Frenkel, "Can stacking faults in hard-sphere crystals anneal out spontaneously?," J. Chem. Phys. **110**, 4589–4592 (1999).
[30]M. Marechal, M. Hermes, and M. Dijkstra, "Stacking in sediments of colloidal hard spheres," J. Chem. Phys. **135**, 034510 (2011).
[31]P. N. Pusey, W. Van Megen, P. Bartlett, B. J. Ackerson, J. G. Rarity, and S. M. Underwood, "Structure of crystals of hard colloidal spheres," Phys. Rev. Lett. **63**, 2753 (1989).
[32]R. van Damme, B. van der Meer, J. J. van den Broeke, F. Smallenburg, and L. Filion, "Phase and vacancy behaviour of hard "slanted" cubes," J. Chem. Phys. **147**, 124501 (2017).
[33]B. van der Meer, R. Van Damme, M. Dijkstra, F. Smallenburg, and L. Filion, "Revealing a vacancy analog of the crowdion interstitial in simple cubic crystals," Phys. Rev. Lett. **121**, 258001 (2018).
[34]F. Smallenburg, L. Filion, M. Marechal, and M. Dijkstra, "Vacancy-stabilized crystalline order in hard cubes," Proc. Natl. Acad. Sci. U. S. A. **109**, 17886–17890 (2012).
[35]H. R. Paneth, "The mechanism of self-diffusion in alkali metals," Phys. Rev. **80**, 708 (1950).
[36]P. M. Derlet, D. Nguyen-Manh, and S. L. Dudarev, "Multiscale modeling of crowdion and vacancy defects in body-centered-cubic transition metals," Phys. Rev. B **76**, 054107 (2007).
[37]D. Nguyen-Manh, A. P. Horsfield, and S. L. Dudarev, "Self-interstitial atom defects in bcc transition metals: Group-specific trends," Phys. Rev. B **73**, 020101 (2006).
[38]Y. N. Osetsky, D. J. Bacon, A. Serra, B. N. Singh, and S. I. Golubov, "One-dimensional atomic transport by clusters of self-interstitial atoms in iron and copper," Philos. Mag. **83**, 61–91 (2003).
[39]S. Han, L. A. Zepeda-Ruiz, G. J. Ackland, R. Car, and D. J. Srolovitz, "Self-interstitials in V and Mo," Phys. Rev. B **66**, 220101 (2002).
[40]L. A. Zepeda-Ruiz, J. Rottler, S. Han, G. J. Ackland, R. Car, and D. J. Srolovitz, "Strongly non-Arrhenius self-interstitial diffusion in vanadium," Phys. Rev. B **70**, 060102 (2004).
[41]T. Kontorova and J. Frenkel, "On the theory of plastic deformation and twinning. II," Z. Eksp. Teor. Fiz. **8**, 1340–1348 (1938).
[42]A. I. Landau, A. S. Kovalev, and A. D. Kondratyuk, "Model of interacting atomic chains and its application to the description of the crowdion in an anisotropic crystal," Phys. Status Solidi B **179**, 373–381 (1993).
[43]A. S. Kovalev, A. D. Kondratyuk, A. M. Kosevich, and A. I. Landau, "Theoretical description of the crowdion in an anisotropic crystal based on the Frenkel-Kontorova model including and elastic three-dimensional medium," Phys. Status Solidi B **177**, 117–127 (1993).
[44]O. M. Braun and Y. S. Kivshar, "Nonlinear dynamics of the Frenkel–Kontorova model," Phys. Rep. **306**, 1–108 (1998).
[45]S. Dudarev, "Coherent motion of interstitial defects in a crystalline material," Philos. Mag. **83**, 3577–3597 (2003).
[46]S. P. Fitzgerald and D. Nguyen-Manh, "Peierls potential for crowdions in the bcc transition metals," Phys. Rev. Lett. **101**, 115504 (2008).
[47]A. Ivlev, G. Morfill, H. Lowen, and C. P. Royall, *Complex Plasmas and Colloidal Dispersions: Particle-Resolved Studies of Classical Liquids and Solids* (World Scientific Publishing Company, 2012), Vol. 5.
[48]D. Frenkel and B. Smit, *Understanding Molecular Simulation: From Algorithms to Applications* (Elsevier, 2001), Vol. 1.
[49]D. Frenkel and A. J. C. Ladd, "New Monte Carlo method to compute the free energy of arbitrary solids. Application to the fcc and hcp phases of hard spheres," J. Chem. Phys. **81**, 3188–3193 (1984).
[50]Note that we have taken the phase boundaries from Ref. 6 and have ensured that the crystal phases do not melt in our simulations.
[51]B. van der Meer, F. Smallenburg, M. Dijkstra, and L. Filion, "High antisite defect concentrations in hard-sphere colloidal laves phases," Soft Matter **16**, 4155 (2020).
[52]J. Tauber, R. Higler, and J. Sprakel, "Anomalous dynamics of interstitial dopants in soft crystals," Proc. Natl. Acad. Sci. U. S. A. **113**, 13660–13665 (2016).